Increased Photovoltaic Power Output via Diffractive Spectrum Separation

Ganghun Kim,[1] Jose A. Dominguez-Caballero,[2] Howard Lee,[3] Daniel J. Friedman,[4] and Rajesh Menon[1,*]

[1]*Department of Electrical and Computer Engineering, University of Utah, Salt Lake City, Utah 84112, USA*

[2]*Department of Mechanical Engineering, Massachusetts Institute of Technology, Cambridge, Massachusetts 02139, USA*

[3]*Stion Corporation, San Jose, California 95119 USA*

[4]*National Renewable Energy Laboratory, Golden, Colorado 80401, USA*

(Received 31 August 2012; published 21 March 2013)

In this Letter, we report the preliminary demonstration of a new paradigm for photovoltaic power generation that utilizes a broadband diffractive-optical element (BDOE) to efficiently separate sunlight into laterally spaced spectral bands. These bands are then absorbed by single-junction photovoltaic cells, whose band gaps correspond to the incident spectral bands. We designed such BDOEs by utilizing a modified version of the direct-binary-search algorithm. Gray scale lithography was used to fabricate these multilevel optics. They were experimentally characterized with an overall optical efficiency of 70% over a wavelength range of 350–1100 nm, which was in excellent agreement with simulation predictions. Finally, two prototype devices were assembled: one with a pair of copper indium gallium selenide based photovoltaic devices, and another with GaAs and *c*-Si photovoltaic devices. These devices demonstrated an increase in output peak electrical power of ~42% and ~22%, respectively, under white-light illumination. Because of the optical versatility and manufacturability of the proposed BDOEs, the reported spectrum-splitting approach provides a new approach toward low-cost solar power.

DOI: 10.1103/PhysRevLett.110.123901 PACS numbers: 42.25.Fx, 73.50.Pz, 88.40.F−, 88.40.hj

Single *p-n* junction photovoltaic devices are fundamentally limited in the efficiency with which they can convert sunlight primarily because photons of energy lower than the band gap are not absorbed, and photons of energy much higher than the band gap lose their excess energy as heat via a process referred to as thermalization [1]. The theoretical maximum efficiency for a single-junction photovoltaic device under unconcentrated sunlight is ~33% [2]. On the other hand, multijunction photovoltaic devices are capable of efficiencies greater than 40% [3,4]. Typically, such devices are vertically stacked junctions, with the band gap of each junction decreasing from top to bottom. The highest energy photons are absorbed at the top junction. Subsequent junctions absorb lower-energy photons. Such devices can be epitaxially grown [4] or mechanically stacked [5]. Mechanically stacked devices can suffer from significant optical losses due to reflections at the interfaces. Epitaxially grown devices suffer from the challenge of fabricating junctions with the combinations of band gaps that are optimal for the solar spectrum. The current produced by each junction must be the same, because the epitaxially grown junctions are typically connected in series. Furthermore, epitaxial devices require a tunnel junction at the interface between each *p-n* junction in the structure, which increases the complexity of the fabrication process. In this Letter, we describe the use of a thin broadband diffractive-optical element (BDOE) designed to efficiently separate and concentrate incident illumination (e.g., sunlight) into predetermined bands that illuminate laterally separated photovoltaic devices of matching band gaps. This approach avoids the aforementioned disadvantages of conventional multijunction devices while utilizing the broad solar spectrum efficiently.

Spectral separation of sunlight may be achieved via refraction, interference, or diffraction [6]. Prisms enable spectral separation via dispersive refraction. However, they are impractical for scaling to large areas due to the volume and weight requirements. Furthermore, they offer very little control over the spatial position of the bands as well as the choices of band edges. Interference, primarily via dichroic and multilayer mirrors, has been used to demonstrate spectral splitting for photovoltaics [7,8]. However, the geometry of such devices precludes scaling to large areas and limits the number of bands that can be separated. Conventional gratings enable spectral separation via diffraction; however, they typically suffer from low diffraction efficiency as well as poor control of the spatial position of the spectral bands.

In contrast, we utilize a nonconventional approach for the design of a multilevel BDOE that spatially separates and concentrates distinct spectral bands as illustrated in Fig. 1(a). We call this BDOE a polychromat. A conventional binary-search algorithm was adapted for the design [9]. This nonlinear optimization algorithm was reformulated to solve a multidimensional constrained problem with an objective function designed to maximize the polychromat's average optical efficiency. The polychromat's optical efficiency at a specific wavelength is defined as the ratio of the radiant energy at that wavelength incident on its optimal absorber divided by the total radiant energy at that wavelength incident on the polychromat. The set of

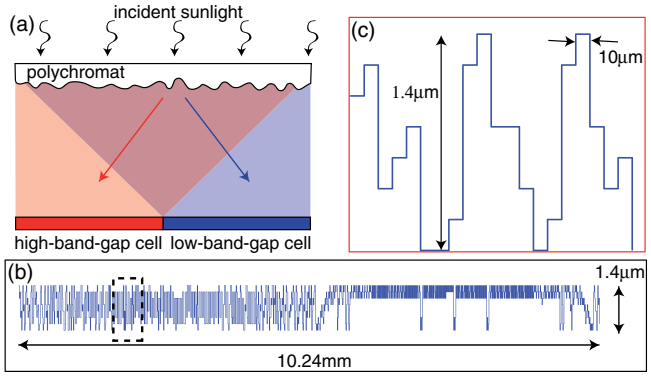

FIG. 1 (color online). (a) A polychromat (a BDOE) separates incident sunlight into two bands, each of which illuminate neighboring solar cells with matched band gaps. (b) An example design of a polychromat represented by the height distribution of its pixels. See text for details. (c) Magnified view of several pixels of the dashed region of the polychromat in (b). Note the eight height levels.

feasible solutions found by the algorithm was constrained to those that matched the required fabrication constraints.

A one-dimensional polychromat that separates sunlight (350–1300 nm) into two bands, 350–800 nm and 801–1100 nm, is shown in Fig. 1(b). The polychromat is comprised of 1000 discrete pixels, each of size 10 μm. On the reconstruction plane, each spectral band covers approximately half the area of the polychromat, corresponding to a concentration factor of $\sim 2\times$. The distance between the polychromat and the reconstruction plane is dictated primarily by diffraction angles and hence, the pixel size. In the current design, the distance was set at 14 cm but it can be reduced to less than 3 cm by choosing a pixel size of 1 μm or smaller [10]. The design was constrained to eight height levels as shown in Fig. 1(b). A magnified view of a selected region is shown in Fig. 1, where the discrete 10 μm-wide pixels as well as eight discrete height levels are apparent.

The polychromat was fabricated using gray scale–optical lithography [11]. An optical micrograph is shown in Fig. 2(a). Figure 2(b) shows a magnified view of an optical profilometer image of a small portion of the same polychromat. The pixels of width 10 μm as well as the multilevel structure are evident. The entire device was comprised of three repeating units in order to account for the assumed periodic boundary conditions, covering an area of about 3×3 cm [10].

The polychromat performance was characterized by measuring the spectrum as a function of position in the reconstruction plane, a spatial-spectral map. Each row in the map corresponds to the spatial distribution of the diffracted light power at the respective wavelength. The measured map is compared against the simulated map in Figs. 2(c) and 2(d). In addition, the measured optical efficiency is compared to the simulated efficiency in Figs. 2(e) and 2(f). The optical efficiency at a given wavelength in the solid blue curve refers to the efficiency with which the photons are allocated to the subcell on the left. The green dashed curve refers to the subcell on the right. The spectrally averaged optical efficiency is 70%. Note that the map and efficiency spectra agree well with the simulations. It must be pointed out that this is the first experimental demonstration of high efficiency ultrabroadband imaging with diffractive optics. Much higher optical efficiencies are expected with more height levels [10].

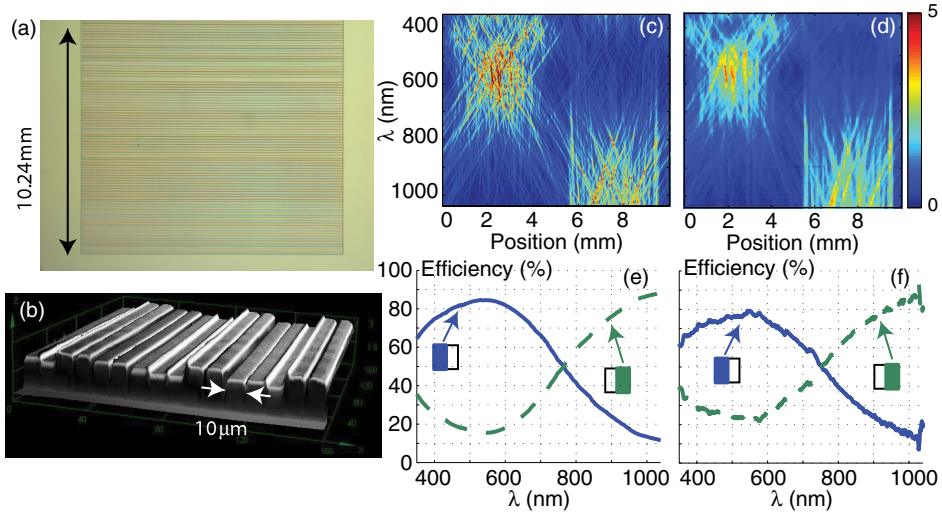

FIG. 2 (color online). (a) Bright-field image of a polychromat. (b) Magnified optical profilograph of a section of the polychromat. Spatial-spectral map at the polychromat reconstruction plane: (c) simulated and (d) measured. Optical efficiency of the polychromat as a function of wavelength: (e) simulated and (f) measured. The solid and dashed curves represent light diverted to the high- and low-band-gap cells, respectively.

We performed electrical characterization with both a pair of copper indium galium selenide (CIGS) cells as well as Si/GaAs cells. The two CIGS cells were designed with band gaps of 1.05 and 1.5 eV. Each cell was placed on a substrate mounted on a single-axis scanning stage with its axis orthogonal to the plane of the polychromat and electrical characteristics measured independently. The distance between the polychromat and the plane containing the cells was set with an optical track to within $+/-1$ mm. The cells were aligned to the spectra visually [10]. Note that in order to achieve sufficient spatial coherence, the light output from the source had to be expanded over a long distance (1.5 m), which resulted in the incident intensity at the polychromat plane being ~4 orders of magnitude smaller than that of the standard AM1.5 spectrum [10]. Under these conditions, the open-circuit voltage is expected to be ~0.25–0.5 V lower than that observed under 1 sun, which is consistent with the measured results shown in Figs. 3 and 4 for CIGS and Si/GaAs cells, respectively. Furthermore, at low illumination intensities, even a small shunt resistance decreases the fill factor significantly (as can be seen for the CIGS cells). The reference measurements are shown as thin red lines, while those with the polychromat are shown as thick blue lines. The polychromat redirects higher-energy photons that would otherwise fall onto the low-band-gap cell (CIGS or Si) to the high-band-gap cell (CIGS or GaAs), and likewise lower-energy photons from the high-band-gap (where they wouldn't be absorbed) to the low-band-gap cell. In other words, the polychromat concentrates input light of each spectral band by a factor of ~2 (the ratio of the area of the polychromat to the area of each cell). For the high-band-gap cell, this results in an increase in short-circuit current density, J_{sc} [Figs. 3(a) and 4(a)]. The increased flux also tends to increase the open-circuit voltage, V_{oc}. Those higher-energy photons that are redirected to the high-band-gap cell are converted to current at a higher voltage than would be the case in the absence of the polychromat; i.e., the low-band-gap cell would have absorbed those photons. As a result, the efficiency of the high-band-gap cell increases with the utilization of the polychromat. On the other hand, the low-band-gap cell loses the higher-energy photons but gains lower-energy photons. Unfortunately, because the halogen lamp used in our experiments had significantly fewer infrared photons compared to visible photons, the total power density of the gained low-energy photons was not sufficient to compensate for the loss of the high-energy photons [10]. As a result, the J_{sc} and V_{oc} both drop slightly for the low-band-gap cell [Figs. 3(b) and 4(b)]. Therefore, a small drop in efficiency of the low-band-gap cell is observed [Figs. 3(d) and 4(d)]. However, this decrease is more than compensated by the increased output power from the high-band-gap cell. Thereby, the total output power density (added

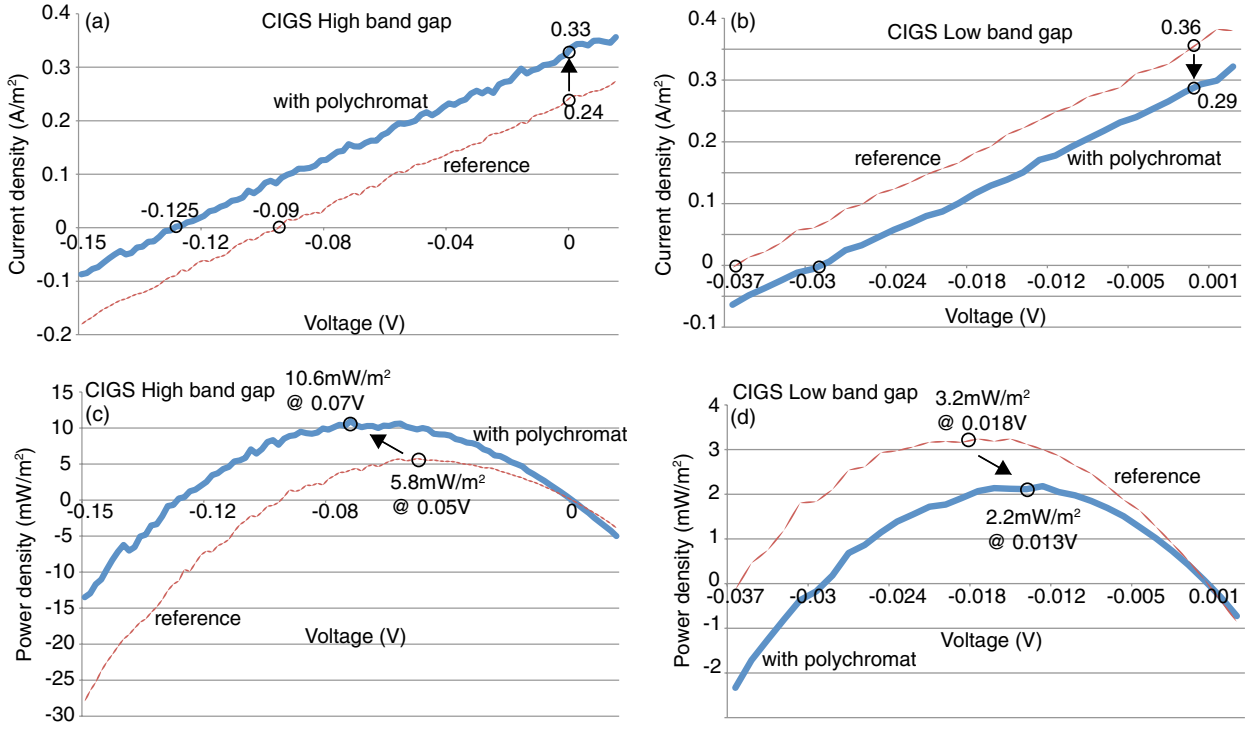

FIG. 3 (color online). Electrical characterization results of CIGS cells. Current density as a function of bias voltage for the high-band-gap (a) and low-band-gap (b) CIGS cells. Power density as a function of bias voltage for the high-band-gap (c) and low-band-gap (d) CIGS cells. The thin red and thick blue curves represent the measurements in the absence of and presence of the polychromat, respectively.

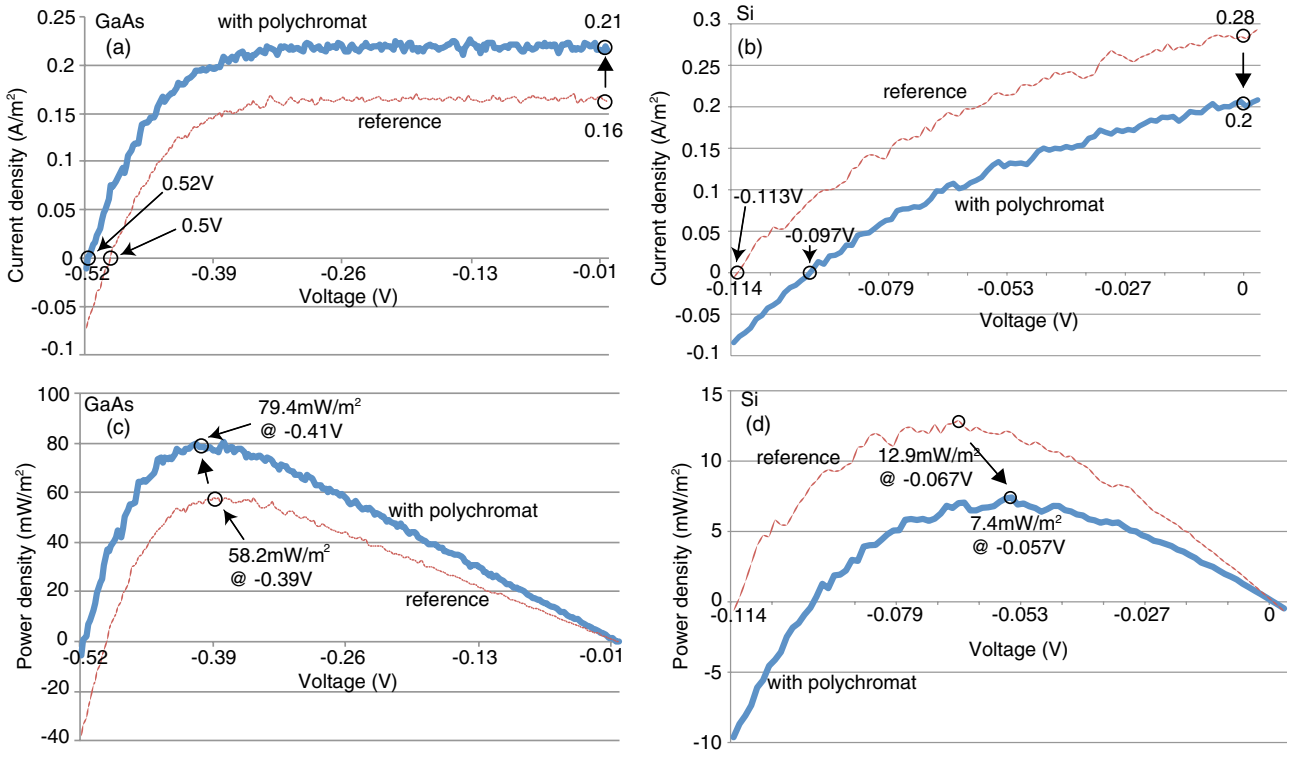

FIG. 4 (color online). Electrical characterization results of GaAs and Si cells. Current density as a function of bias voltage for the GaAs (a) and Si (b) cells. Power density as a function of bias voltage for the GaAs (c) and Si (d) cells. The thin red and thick blue curves represent the measurements in the absence of and presence of the polychromat, respectively.

from both cells) with the polychromat is increased by ~42% for CIGS [Fig. 3(c)] and ~22% for Si/GaAs [Fig. 4(c)].

Numerical simulations indicate that ideal spectrum splitting with these pairs of cells can result in an increase in output power density of ~68% [10]. Much of the discrepancy with the measured results can be accounted for by the decrease in the polychromat efficiency close to the band edge and the low illumination level. The results as well as other simulations that assume AM1.5 [10] incident spectrum suggest that an integrated design approach for the polychromat that takes into account the cell performance under specific illumination conditions could achieve power-density increases that are closer to the theoretical limits. Nevertheless, our initial results clearly indicate the potential of using a polychromat for efficient spectrum splitting.

BDOEs may be designed to separate more than two bands, allowing for even higher conversion efficiencies. Another interesting advantage of this approach is that by avoiding the thermalization losses in the low-band-gap subcell, we could reduce its temperature. In our preliminary experiments, the polychromat covered only a small area (3 × 3 cm). For a practical photovoltaic system, the area must be scaled to ~1 × 1 m. This is possible in a cost-effective manner with manufacturing methods such as roll-to-roll processing [12]. Although III–V materials such as GaAs are currently too expensive to use under low or no concentration, recent advances in thin-film GaAs manufacturing [13] are rapidly decreasing costs and the proposed spectrum-splitting approaches can play a major role in achieving high-photovoltaic-system efficiencies with only a marginal increase in costs.

We thank Jim Daley, Brian Van Devener, Kevin Hensley, and Brian Baker for assistance with microfabrication and imaging. We thank Sarah Kurtz for assistance with the development of the GaAs cells. We acknowledge assistance during electrical measurements from Ye Zhang. We thank Keith Emery for useful discussion of the results. G. K. was partially supported by a Technology Commercialization Grant from the University of Utah Research Foundation. R. M. acknowledges funding from the Utah Science Technology and Research (USTAR) Initiative. D. F. was supported by the US DOE under Contract No. DE-AC36-08GO28308 with NREL.

*To whom all correspondence should be addressed.
rmenon@eng.utah.edu

[1] C. H. Henry, J. Appl. Phys. **51**, 4494 (1980).
[2] O. D. Miller, E. Yablonovitch, and S. R. Kurtz, IEEE J. Photovolt. **2**, 303 (2012).
[3] J. F. Geisz, D. J. Friedman, J. S. Ward, A. Duda, W. J. Olavarria, T. E. Moriatry, J. T. Kiehl, M. J. Romero,

A. G. Norman, and K. M. Jones, Appl. Phys. Lett. **93**, 123505 (2008).
[4] R. R. King, D. C. Law, K. M. Edmondson, C. M. Fetzer, G. S. Kinsey, H. Yoon, R. A. Sherif, and N. H. Karam, Appl. Phys. Lett. **90**, 183516 (2007).
[5] L. M. Fraas, J. E. Avery, J. Martin, V. S. Sundaram, G. Girard, V. T. Dinh, T. M. Davenport, J. W. Yerkes, and V. S. O'Neil, IEEE Trans. Electron Devices **37**, 443 (1990).
[6] A. G. Imenes and D. R. Mills, Solar Energy Mater. Sol. Cells **84**, 19 (2004).
[7] B. Mitchell, G. Peharz, G. Siefer, M. Peters, T. Gandy, J. G. Goldschmidt, J. Benick, S. W. Glunz, A. W. Bett, and F. Dimroth, Prog. Photovoltaics **19**, 61 (2011).
[8] A. Barnett *et al.*, Prog. Photovoltaics **17**, 75 (2009).
[9] G. Kim, J.-A. Dominguez-Caballero, and R. Menon, Opt. Express **20**, 2814 (2012).
[10] See Supplemental Material at http://link.aps.org/supplemental/10.1103/PhysRevLett.110.123901 for the details of the design, fabrication and characterization of the polychromat and the assembled devices.
[11] U. Levy, B. Desiatov, I. Goykhman, T. Nachmias, A. Ohayon, and S. E. Meltzer, Opt. Lett. **35**, 880 (2010).
[12] S. H. Ahn and L. J. Guo, Adv. Mater. **20**, 2044 (2008).
[13] See cells from Alta Devices listed in M. A. Green, K. Emery, Y. Hishikawa, W. Warta, and E. D. Dunlop, Prog. Photovoltaics **19**, 565 (2011).